atoms

IMPACT FACTOR 1.7

CITESCORE 2.7

Article

Informational Entropy Analysis of Artificial Helium Atoms

Marcilio N. Guimarães, Rafael N. Cordeiro, Wallas S. Nascimento and Frederico V. Prudente

MDPI

https://doi.org/10.3390/atoms13050042

atoms

MDPI

Article

Informational Entropy Analysis of Artificial Helium Atoms

Marcilio N. Guimarães [†], Rafael N. Cordeiro [†], Wallas S. Nascimento [†] and Frederico V. Prudente [*,†]

Instituto de Física, Universidade Federal da Bahia, Salvador 40170-110, BA, Brazil; mng@ufba.br (M.N.G.); arcanjorafael2@gmail.com (R.N.C.); wallassantos@gmail.com (W.S.N.)

* Correspondence: prudente@ufba.br

† These authors contributed equally to this work.

Abstract: We use the Shannon informational entropies as a tool to study the artificial helium atom, namely, two electrons confined in a quantum dot. We adopt configurations with spherical and cylindrical symmetries for the physical system of interest. Using the informational quantities, we analyze the effects of electronic confinement, we validate the entropic uncertainty relation, we identify that the Coulomb interaction potential between the electrons is no longer important for strong confinements, and we indicate/predict the avoided crossing phenomena. Finally, we carried out a density function analysis. When available, the results are compared with those in the literature.

Keywords: artificial atoms; quantum-dot helium; Shannon entropy; avoided crossing

1. Introduction

The study of nanostructures such as quantum dots has attracted the attention of researchers due to their promising technological applications [1]. The fact that we can alter the properties of quantum dots makes these structures useful in the manufacture of devices such as transistors [2,3], solar cells [4,5], LEDs [6,7], etc. In the context of quantum computing, quantum dots are treated as possible qubit candidates [8,9].

Quantum dots are conductive regions of the order of De Broglie wavelength located in a semiconductor. A quantum dot can be formed by the junction of two semiconductors with different energy band gaps that form heterostructures with certain conduction bands. In turn, such bands form a quantum well of finite potential that can confine charge carriers [10,11]. Quantum dots can be modeled as artificial atoms, with the electrons contained in these nanostructures being confined in the three spatial directions, ($\widehat{x}$, $\widehat{y}$ and $\widehat{z}$), and have well-defined discrete quantum states [12,13]. Nevertheless, in the literature we find comparative investigations between quantum dots treated as artificial atoms and real atoms [14].

In the context of spatially confined quantum systems, we find several studies on quantum dots [15,16]. The quantum dot is an extremely manipulable structure, so we can, for example, undertake analyses on the number of electrons that can be confined in this nanostructure, [17,18], as well as investigations on how the size [19,20] and different confinement potentials [21,22] can affect the properties of such a system. Furthermore, interesting results are obtained when these nanostructures, which have confinement effects, are crossed by a laser field [23,24] or a magnetic field [25,26].

Historically, information or entropic measures were introduced into the quantum mechanics context for the characterization of the degree of mixedness of quantum mixed states. Studies indicate how entropic measures of information can be used in connection with quantum pure states in quantum mechanics (see, for instance, Ref. [27] and references

Academic Editor: Gordon W. F. Drake

Received: 27 February 2025
Revised: 25 April 2025
Accepted: 3 May 2025
Published: 12 May 2025

Citation: Guimarães, M.N.; Cordeiro, R.N.; Nascimento, W.S.; Prudente, F.V. Informational Entropy Analysis of Artificial Helium Atoms. *Atoms* **2025**, *13*, 42. https://doi.org/10.3390/atoms13050042

therein). On the other hand, the Shannon informational entropy initially appears in the field of information theory [28,29]. This informational measure has been applied in different fields of knowledge [30,31] and, in particular, has been successfully used in the field of atomic and molecular physics [32,33].

In the treatment of confined quantum systems, Shannon entropy has been applied in several studies involving, for example, confined hydrogen [34–36] and helium atoms [37–39], in addition to plasma systems [40,41]. Recent work indicates the possibility of using informational quantities in the treatment of quantum dots [42–45].

In systems such as quantum dots, there is the possibility of the occurrence of the avoided crossings phenomenon. This phenomenon is characterized by the energy values of different states coming very close together without becoming equal and then moving away from each other. Neighboring energy levels with the same symmetry do not intersect. Pioneering studies involving hydrogen atom in the presence of the uniform magnetic and electric fields indicate that Shannon and Fisher entropies are good predictors of avoided crossings [46,47].

The aim of this work is to investigate, through Shannon informational entropies, the motion of two electrons confined by a three-dimensional harmonic potential (isotropic and anisotropic cases) in a quantum dot. In this sense, we implement computational numerical procedures based on the finite element approximation to determine the optimized variational wave function and, subsequently, obtain the values of the entropic quantities of interest.

This work is divided as follows: In Section 2 we present the theoretical background in which we mathematically formulate the problem of the two-electron quantum dot atom, known as the artificial helium atom, and obtain Shannon informational entropies. In Section 3 we present the results for the computations of the entropies for the cases in which the confinement potential is isotropic (spherical artificial helium) and anisotropic (cylindrical artificial helium). Finally, in Section 4 we present the conclusions and perspectives.

2. Theoretical Background

In this section, we present as the physical system of interest the artificial helium atom in its spherical and cylindrical configurations. In particular, we highlight the descriptions of this system in the coordinates of the center of mass and of the relative motion between the two electrons (Section 2.1). Besides, we define the Shannon informational entropies (Section 2.2). We develop all the formalism of this section using effective atomic units ($\hbar = m_e^* = e/\sqrt{\kappa} = 1$).

2.1. System of Interest

The artificial helium atom is defined as a system of two electrons confined in a quantum dot described by the following Hamiltonian:

$$\widehat{H} = \sum_{i=1}^{2}\left[\frac{1}{2}\mathbf{p}_i^2 + V_{dot}(\mathbf{r}_i)\right] + \frac{1}{|\mathbf{r}_1 - \mathbf{r}_2|}\,, \tag{1}$$

where $\mathbf{r}_i$ and $\mathbf{p}_i$ are the position and generalized momentum vectors, respectively, of the i-th particle. In this work, we adopted a three-dimensional harmonic confinement potential, V_{dot}, given by,

$$V_{dot}(\mathbf{r}_i) = \frac{1}{2}\left[\omega_\perp^2\left(x_i^2 + y_i^2\right) + \omega_z^2 z_i^2\right]\,, \tag{2}$$

where the angular frequencies $\omega_\perp$, in the XY-plane, and ω_z, in the Z-direction, are confinement parameters. In the case in which $\omega_\perp = \omega_z$ (isotropic case of the potential), the confinement potential has a spherical symmetry, characterizing a spherical artificial helium

atom. When $\omega_\perp \neq \omega_z$ (anisotropic case of the potential), the confinement potential has a cylindrical symmetry, defining the cylindrical artificial helium atom.

The present problem allows that the Hamiltonian, $\widehat{H}$, to be separated into a contribution involving only the coordinates of the center of mass ($\mathbf{R} = (\mathbf{r_1} + \mathbf{r_2})/2$), $\widehat{H}_{CM}$, and another referring to the relative motion coordinate between the two electrons ($\mathbf{r} = \mathbf{r_1} - \mathbf{r_2}$), $\widehat{H}_{RM}$, such that,

$$\widehat{H} = \widehat{H}_{CM} + \widehat{H}_{RM} \, . \tag{3}$$

In this scenario, the total solution wavefunction, $\Psi(\mathbf{R}, \mathbf{r})$, for $\widehat{H}$, and its Fourier transform, $\widetilde{\Psi}(\mathbf{P}, \mathbf{p})$, can be separable into a two-part product, that is,

$$\Psi(\mathbf{R}, \mathbf{r}) = \Psi_{CM}(\mathbf{R}) \cdot \Psi_{RM}(\mathbf{r}) \quad \text{and} \quad \widetilde{\Psi}(\mathbf{P}, \mathbf{p}) = \widetilde{\Psi}_{CM}(\mathbf{P}) \cdot \widetilde{\Psi}_{RM}(\mathbf{p}), \tag{4}$$

where $\Psi_{CM}(\mathbf{R})$ and $\Psi_{RM}(\mathbf{r})$ are the solution wavefunctions for $\widehat{H}_{CM}$ and $\widehat{H}_{RM}$, respectively. Furthermore, $\widetilde{\Psi}_{CM}(\mathbf{P})$ and $\widetilde{\Psi}_{RM}(\mathbf{p})$ are the appropriate momentum space wavefunction. In turn, the total energy, E, is given by

$$E = E_{CM} + E_{RM} \, . \tag{5}$$

As we will analyze below, the problem concerning the center of mass motion has an analytical solution. However, the problem of the relative motion between the two electrons cannot be solved analytically, so we will reduce the problem to a one-dimensional equation in the radial variable that will be resolved using the finite element method (FEM).

2.1.1. Center of Mass Motion

The Hamiltonian of the center of mass motion is

$$\widehat{H}_{CM} = -\frac{1}{4}\nabla^2_{\mathbf{R}} + \omega_\perp^2 \left(X^2 + Y^2\right) + \omega_z^2 Z^2 \, , \tag{6}$$

where $\nabla_{\mathbf{R}}$ is the Laplacian operator. The time-independent Schrödinger equation referring to $\widehat{H}_{CM}$ has an exact solution, being the solution wavefunctions in the space of positions, $\Psi_{CM}(\mathbf{R})$, and momentum, $\widetilde{\Psi}_{CM}(\mathbf{P})$, in cylindrical coordinates, written as

$$\Psi_{CM}(\mathbf{R}) = \mathcal{R}(R)\mathcal{O}(\Phi)\mathcal{Z}(Z) \quad \text{and} \quad \widetilde{\Psi}_{CM}(\mathbf{P}) = \widetilde{\mathcal{R}}(P_R)\widetilde{\mathcal{O}}(P_\Phi)\widetilde{\mathcal{Z}}(P_Z) \, , \tag{7}$$

with

$$\mathcal{R}(R) = \sqrt{\frac{2 \cdot N!}{(N + |M|)!}} \, \overline{\omega}_\perp^{\frac{|M|+1}{2}} \cdot e^{-\frac{\overline{\omega}_\perp}{2}R^2} \cdot R^{|M|} \cdot \mathcal{L}_N^{|M|}\left(\overline{\omega}_\perp R^2\right) \tag{8}$$

$$\mathcal{O}(\Phi) = \frac{1}{\sqrt{2\pi}} e^{iM\Phi} \tag{9}$$

$$\mathcal{Z}(Z) = \sqrt{\frac{1}{2^{N_Z} N_Z!}} \left(\frac{\overline{\omega}_z}{\pi}\right)^{\frac{1}{4}} \cdot e^{-\frac{\overline{\omega}_z}{2}Z^2} \cdot \mathcal{H}_{N_Z}\left(\sqrt{\overline{\omega}_z} Z\right), \tag{10}$$

where, $\overline{\omega}_\perp = 2\omega_\perp$ and $\overline{\omega}_z = 2\omega_z$. On the other hand, we have

$$\widetilde{\mathcal{R}}(P_R) = \sqrt{\frac{2 \cdot N!}{(N + |M|)!}} \, \widetilde{\omega}_\perp^{\frac{|M|+1}{2}} \cdot e^{-\frac{\widetilde{\omega}_\perp}{2}P_R{}^2} \cdot P_R{}^{|M|} \cdot \mathcal{L}_N^{|M|}\left(\widetilde{\omega}_\perp P_R{}^2\right) \tag{11}$$

$$\widetilde{\mathcal{O}}(P_\Phi) = \frac{1}{\sqrt{2\pi}} e^{iMP_\Phi} \tag{12}$$

$$\widetilde{\mathcal{Z}}(P_Z) = \sqrt{\frac{1}{2^{N_Z} N_Z!}} \left(\frac{\widetilde{\omega}_z}{\pi}\right)^{\frac{1}{4}} \cdot e^{-\frac{\widetilde{\omega}_z}{2}P_Z{}^2} \cdot \mathcal{H}_{N_Z}\left(\sqrt{\widetilde{\omega}_z} P_Z\right), \tag{13}$$

being that $\widetilde{\omega}_\perp = 1/2\omega_\perp$ and $\widetilde{\omega}_z = 1/2\omega_z$. The functions $\mathcal{H}_{N_Z}$ and $\mathcal{L}_N^{|M|}$ are the Hermite and associated Laguerre polynomials, respectively.

In turn, the energy eigenvalues are written exactly as

$$E_{CM} = (2N + |M| + 1)\omega_\perp + \left(N_Z + \frac{1}{2}\right)\omega_z \,, \tag{14}$$

where N and M are, respectively, the radial and the azimuthal quantum numbers associated with the XY-planar oscillator. Furthermore, N_Z is the quantum number associated with the Z-direction harmonic oscillator.

2.1.2. Relative Motion Between the Two Electrons

The Hamiltonian of the relative motion between the two electrons is

$$\widehat{H}_{RM} = -\nabla_{\mathbf{r}}^2 + \frac{1}{4}\omega_\perp^2\left(x^2 + y^2\right) + \frac{1}{4}\omega_z^2 z^2 + \frac{1}{r} \,, \tag{15}$$

where $\nabla_{\mathbf{r}}$ is the Laplacian operator and $r = |\mathbf{r}_1 - \mathbf{r}_2|$. The time independent Schrödinger equation referring to $\widehat{H}_{RM}$ cannot be solved analytically due to the Coulomb interaction $(1/r)$. In order to solve it, we first expand the wavefunctions in the space of positions, $\Psi_{RM}(\mathbf{r})$, and momentum, $\widetilde{\Psi}_{RM}(\mathbf{p})$, in a product of spherical harmonics and radial functions, so that,

$$\Psi_{RM}(\mathbf{r}) = \sum_l Y_l^m(\theta,\phi)\cdot\frac{\varphi_{lm}(r)}{r} \quad \text{and} \quad \widetilde{\Psi}_{RM}(\mathbf{p}) = \sum_l Y_l^m(p_\theta,p_\phi)\cdot\frac{\widetilde{\varphi}_{lm}(p_r)}{p_r}, \tag{16}$$

where l and m are the polar and azimuthal quantum numbers. The radial function in momentum space is written as

$$\widetilde{\varphi}_{lm}(p_r) = (-i)^l\sqrt{\frac{2}{\pi}}\int \mathcal{J}_l(p_r r)\varphi_{lm}(r)\; p_r r\; dr \,, \tag{17}$$

where $\mathcal{J}_l$ are the spherical Bessel functions.

Based on variational formalism, the relative motion problem turns out to be the solution of an eigenvalue-eigenvector problem. To obtain this, the radial function, φ_{lm}, is expanded in a set of base functions $\{f_j(r)\}$ with coefficients $\{c_j\}$, obtaining the following

$$\mathbf{Hc} = E_{RM}\mathbf{Oc} \,, \tag{18}$$

where $\mathbf{c}$ is the coefficient vector,

$$\begin{aligned}\{\mathbf{H}\}_{ij}^{ll'} = \int dr\Bigg\{&\left[\frac{df_i^*(r)}{dr}\frac{df_j(r)}{dr} + f_i^*(r)V_l^{ef}(r)f_j(r)\right]\delta_{ll'} \\ &+\frac{\Delta\omega^2}{4}f_i^*(r)r^2 f_j(r)\cdot A_{ll'}^m\Bigg\}\end{aligned} \tag{19}$$

and

$$\{\mathbf{O}\}_{ij}^{ll'} = \int dr f_i^*(r)f_j(r)\cdot\delta_{ll'} \,. \tag{20}$$

with $V_l^{ef}(r) = l(l+1)/r^2 + \omega_\perp^2 r^2/4 + 1/r$, $\Delta\omega^2 = \omega_z^2 - \omega_\perp^2$ and

$$\begin{aligned} A_{ll'}^m &= \left[\frac{(l-m+1)(l+m+1)(l-m+2)(l+m+2)}{(2l+1)(2l+3)^2(2l+5)}\right]^{\frac{1}{2}} \delta_{l',l+2} + \\ &\left[\frac{(l-m+1)(l+m+1)}{(2l+1)(2l+3)} + \frac{(l-m)(l+m)}{(2l-1)(2l+1)}\right]\delta_{l',l} + \\ &\left[\frac{(l-m)(l+m)(l-m-1)(l+m-1)}{(2l+1)(2l-1)^2(2l-3)}\right]^{\frac{1}{2}} \delta_{l',l-2}\,, \end{aligned} \tag{21}$$

wherein the coupling terms, $A_{ll'}^m$, imposes the condition that the whole set of values of l (and l') must be either even (singlet state) or odd (triplet state).

The function expansion method we employed to generate the base functions, $\{f_j(r)\}$, and to solve the generalized eigenvalue-eigenfunction problem of Equation (18), obtaining the energies, E_{RM}, and coefficients of expansion, $\{c_j\}$, from the radial function, was the one-dimensional finite element method. It consists of dividing the range of integration into elements and using locally defined polynomial base functions (see reference [48] for details).

Here, exclusively, in terms of nomenclature/notation, we adopted the quantum numbers in the context of the problem without considering the Coulomb interaction between the electrons. In fact, when we suppress the term $(1/r)$ from Hamiltonian (15), we have the problem of two electrons without interaction. In this case, the energy of the relative motion between the two electrons is given by

$$E_{RM}^{non} = (2n + |m| + 1)\omega_\perp + \left(n_Z + \frac{1}{2}\right)\omega_z. \tag{22}$$

Thus, the quantum numbers associated with relative motion are n, m and n_z with similar meanings to the ones in expression (14). Anyway, as we will see in the results section, the calculations of E_{RM} will be numerical.

2.2. Shannon Informational Entropies

In the atomic and molecular physics context, the Shannon informational entropies in the spaces of positions, S_r, and momentum, S_p, are defined as [36,49]

$$S_r = -\int |\Psi(\mathbf{R},\mathbf{r})|^2 \, \ln\Big(\, |\Psi(\mathbf{R},\mathbf{r})|^2\Big)\, d\mathbf{R}d\mathbf{r} \tag{23}$$

and

$$S_p = -\int |\widetilde{\Psi}(\mathbf{P},\mathbf{p})|^2 \, \ln\Big(\, |\widetilde{\Psi}(\mathbf{P},\mathbf{p})|^2\Big)\, d\mathbf{P}d\mathbf{p}\,, \tag{24}$$

where $\Psi(\mathbf{R},\mathbf{r})$ and $\widetilde{\Psi}(\mathbf{P},\mathbf{p})$ are the wavefunctions in position and momentum spaces (both normalized the unit), respectively. The S_r and S_p quantities are measures of uncertainty, localization or delocalization, of the wavefunction in the space [50,51]. Adding the Equations (23) and (24) we obtain the entropy sum $S_t = S_r + S_p$, from where we can derive the following entropic uncertainty relation [52]

$$S_t \geq D\,(1 + \ln \pi)\,, \tag{25}$$

where D is the dimension of the system.

Employing the Equation (4) in (23) and (24) we can write the S_r and S_p entropies as

$$S_r = S_{CM} + S_{RM} \quad \text{and} \quad S_p = \widetilde{S}_{CM} + \widetilde{S}_{RM}\,, \tag{26}$$

with

$$S_{CM} = -\int |\Psi_{CM}(\mathbf{R})|^2 \ln\left(|\Psi_{CM}(\mathbf{R})|^2\right) d\mathbf{R} \quad \text{and} \quad \widetilde{S}_{CM} = -\int |\widetilde{\Psi}_{CM}(\mathbf{P})|^2 \ln\left(|\widetilde{\Psi}_{CM}(\mathbf{P})|^2\right) d\mathbf{P}\,, \tag{27}$$

furthermore,

$$S_{RM} = -\int |\Psi_{RM}(\mathbf{r})|^2 \ln\left(|\Psi_{RM}(\mathbf{r})|^2\right) d\mathbf{r} \quad \text{and} \quad \widetilde{S}_{RM} = -\int |\widetilde{\Psi}_{RM}(\mathbf{p})|^2 \ln\left(|\widetilde{\Psi}_{RM}(\mathbf{p})|^2\right) d\mathbf{p}. \tag{28}$$

Considering that the wavefunction of the center of mass is separable as shown by the expressions in (7), then, by the expressions in (27), we have

$$S_{CM} = S_R + S_\Phi + S_Z \quad \text{and} \quad \widetilde{S}_{CM} = S_{P_R} + S_{P_\Phi} + S_{P_Z}, \tag{29}$$

with

$$S_R = -\int |\mathcal{R}(R)|^2 \ln\left(|\mathcal{R}(R)|^2\right) RdR \tag{30}$$

$$S_\Phi = -\int |\mathcal{O}(\Phi)|^2 \ln\left(|\mathcal{O}(\Phi)|^2\right) d\Phi \tag{31}$$

$$S_Z = -\int |\mathcal{Z}(Z)|^2 \ln\left(|\mathcal{Z}(Z)|^2\right) dZ \tag{32}$$

where $\mathcal{R}(R)$, $\mathcal{O}(\Phi)$ and $\mathcal{Z}(Z)$ functions are given by the Equations (8), (9) and (10), respectively. And

$$S_{P_R} = -\int |\widetilde{\mathcal{R}}(P_R)|^2 \ln\left(|\widetilde{\mathcal{R}}(P_R)|^2\right) P_R dP_R \tag{33}$$

$$S_{P_\Phi} = -\int |\widetilde{\mathcal{O}}(P_\Phi)|^2 \ln\left(|\mathcal{O}(\Phi)|^2\right) dP_\Phi \tag{34}$$

$$S_{P_Z} = -\int |\widetilde{\mathcal{Z}}(P_Z)|^2 \ln\left(|\widetilde{\mathcal{Z}}(P_Z)|^2\right) dP_Z\,, \tag{35}$$

being that $\widetilde{\mathcal{R}}(P_R)$, $\widetilde{\mathcal{O}}(P_\Phi)$ and $\widetilde{\mathcal{Z}}(P_Z)$ are given by the Equations (11), (12) and (13), respectively.

The wavefunction of the relative motion between the electrons, given by Equation (16), is not separable for any value of l, then, by expressions in (28), we have,

$$S_{RM} = -2\pi \iint \sum_{ll'} \mathcal{N}_l^m \mathcal{P}_l^m(\theta) \mathcal{N}_{l'}^m \mathcal{P}_{l'}^m(\theta) \cdot \varphi_{lm}(r)\varphi_{l'm}(r) \cdot \ln\left(\sum_{ll'} \mathcal{N}_l^m \mathcal{P}_l^m(\theta) \mathcal{N}_{l'}^m \mathcal{P}_{l'}^m(\theta) \frac{\varphi_{lm}(r)\varphi_{l'm}(r)}{r^2}\right) \sin\theta \; drd\theta \tag{36}$$

and

$$\widetilde{S}_{RM} = -2\pi \iint \sum_{ll'} \mathcal{N}_l^m \mathcal{P}_l^m(p_\theta) \mathcal{N}_{l'}^m \mathcal{P}_{l'}^m(p_\theta) \cdot \widetilde{\varphi}_{lm}(p_r)\widetilde{\varphi}_{l'm}(p_r) \cdot \ln\left(\sum_{ll'} \mathcal{N}_l^m \mathcal{P}_l^m(p_\theta) \mathcal{N}_{l'}^m \mathcal{P}_{l'}^m(p_\theta) \frac{\widetilde{\varphi}_{lm}(p_r)\widetilde{\varphi}_{l'm}(p_r)}{p_r^2}\right) \sin p_\theta \; dp_r dp_\theta, \tag{37}$$

where $\mathcal{N}_l^m = (-1)^m \sqrt{[(2l+1)(l-m)!]/[4\pi(l+m)!]}$ and $\mathcal{P}_l^m$ are associated Legendre polynomials.

In general, taking into account the problems of the center of mass and relative motion between the electrons, the entropy sum, S_t, is

$$\begin{aligned} S_t =& S_{CM} + S_{RM} + \widetilde{S}_{CM} + \widetilde{S}_{RM} \\ S_t =& S_R + S_\Phi + S_Z + S_{RM} + S_{P_R} + S_{P_\Phi} + S_{P_Z} + \widetilde{S}_{RM}. \end{aligned} \tag{38}$$

The Shannon informational entropies are dimensionless quantities from the point of view of physics. A detailed discussion about this topic can be found in the Refs. [36,50].

3. Results

In this section, we present and discuss the values of the S_r and S_p entropies (expressions in (26)) and of the entropy sum S_t (expressions in (38)) for the spherical and cylindrical artificial helium atoms in different quantum number configurations. The integrals S_R, S_Z, S_{RM}, S_{P_R}, S_{P_Z} and $\widetilde{S}_{RM}$ are solved by Gauss–Laguerre, Gauss–Hermite and Gauss–Legendre quadrature integrations. Furthermore, we determined that $S_\Phi = S_{P_\Phi} = \ln(2\pi)$.

In particular, the convergence of numerical calculations of integrations S_{RM} and $\widetilde{S}_{RM}$ was tested by the normalization condition

$$\int |\Psi_{RM}(\mathbf{r})|^2 d\mathbf{r} = 1 \quad \text{and} \quad \int |\widetilde{\Psi}_{RM}(\mathbf{p})|^2 d\mathbf{p} = 1\,. \tag{39}$$

In fact, they used different position and momentum radial mesh ranges in numerical integrations due to the fact that when there is a lower dispersion of the radial function a smaller mesh size is needed so that we can use an sufficient number of points for numerical integration in the region where the function was not null and, consequently, ensure the condition of normalization of the Equation (39).

We also determined the total energy, E, for the physical system of interest using the Equation (5). E_{CM} is obtained by Equation (14) and E_{RM} using the numerical method we present in the Section 2.1. All our calculations were performed using a computational implementation in Fortran and utilizing the effective atomic units.

In order to assess the reliability, we compared our results for relative motion energies, for some values of potential parameter, with the accurate ones from Prudente et al. [53] calculated using the discrete variable representation method (DVR). Our calculation with FEM was performed by making an equidistant discretization with $N_e = 20$ mesh elements, $k = 5$ maximum polynomial order and up to 20 spherical harmonics with a particular symmetry (l even or odd) while the DVR utilized 100 base functions and 30 spherical harmonics. At virtually all the levels compared, our results agreed perfectly down to the fifth decimal place. Therefore, we consider that our numerical basis functions are satisfactory.

3.1. Spherical Artificial Helium Atom

First, we investigate the spherical artificial helium atom (isotropic situation of the potential). In this case, making $\omega = \omega_\perp = \omega_z$ in Equation (14) we have

$$E_{CM} = \left(2N + L + \frac{3}{2}\right)\omega\,. \tag{40}$$

Additionally, from Equation (22) we found that

$$E_{RM}^{non} = \left(2n + l + \frac{3}{2}\right)\omega\,. \tag{41}$$

So, the states for the motion of the center of mass and of the relative motion between the electrons are defined by the quantum numbers (N, L) and (n, l), respectively. In addition, we have $L = |M| + N_Z$ and we identify a decoupling in angular momentum l ($\Delta\omega = 0$ in Equation (19)) from which it follows $l = |m| + n_Z$.

We present all the results obtained for the total energy, E, and the S_r, S_p and S_t entropies for different states, (n, l), but always in the ground state of the center of mass problem, i.e., $(N, L) = (0, 0)$.

In Figure 1 we have the total energy, E, for different quantum states, (n, l), as a function of ω. It can be observed that the thin band structure appears when the confinement situation increases with the increase in the ω values. In fact, for large values of ω the influence of the Coulomb correlation of repulsion on the electrons is smaller and their movements begin to be mainly governed by the harmonic confinement potential, whose associated energy spectrum has degeneracies for some values of n and l, as seen in the expression (41). No avoided crossing is noticed, apparently, this is due to the spherical symmetry of the potential.

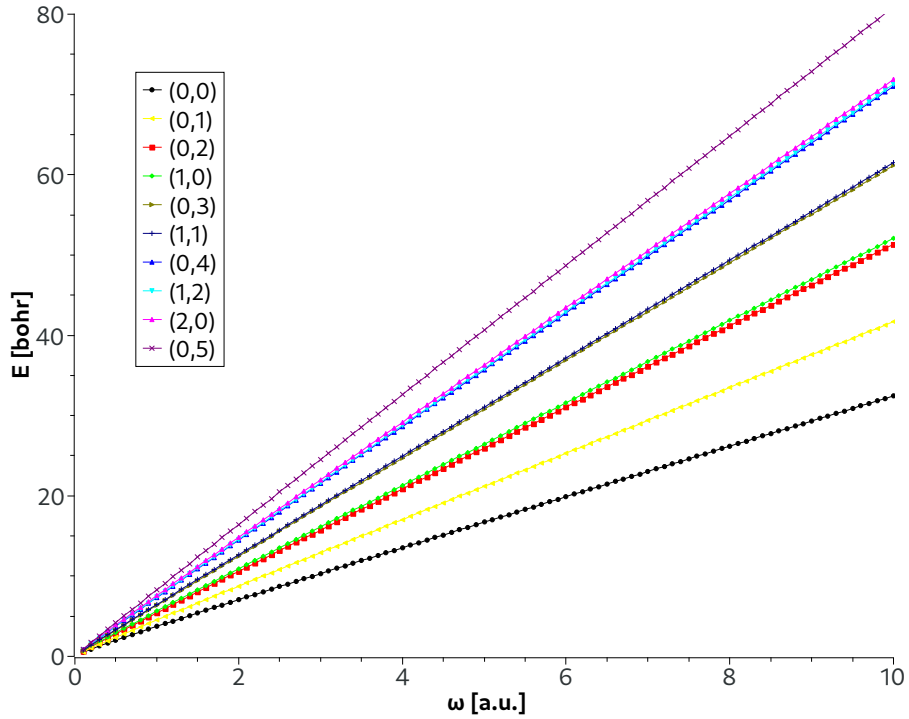

Figure 1. Total energy, E, for different quantum states, (n, l), as a function of ω for the spherical artificial helium atom.

In Table 1 we present the results for the informational entropy in the position space obtained by Cordeiro [54] and by the present work. Cordeiro [54] shows results for the ground and first excited states, $(n, l) = (0, 0)$ and $(1, 0)$, respectively, also with $(N, L) = (0, 0)$. His calculation was performed using a method based in a set of hyperspherical coordinates making a separation between the hyperradius and the hyperangles, similarly to the separation adiabatic between nuclear and electronic coordinates for a molecule, and solving differential equations using FEM. We have a good agreement between the results obtained by Cordeiro [54] and by the present work, thus ensuring the reliability of our results.

Table 1. Informational entropy S_r for the ground, (0, 0), and first excited states, (1, 0), with different ω values for the spherical artificial helium atom.

	S_r			
	$(0,0)$		$(1,0)$	
ω	**Cordeiro [54]**	**Present**	**Cordeiro [54]**	**Present**
0.1	14.1560	14.1564	14.7033	14.7037
0.25	11.1877	11.1880	11.8127	11.8137
0.5	8.9695	8.9697	9.6539	9.6545
1.0	6.7766	6.7767	7.5157	7.5168
4.0	2.4600	2.4599	3.2836	3.2836

In Figure 2, in graphs (a) and (b), respectively, we have the values of informational entropies in the spaces of positions, S_r, and momentum, S_p, for different system states, (n, l), as a function of ω. In graph (c) we present the curves of S_t versus ω. As expected, S_r decreases with increasing confinement intensity (increasing ω values), on the other hand, the S_p increases with increasing ω. This means that as the confinement becomes more intense, the uncertainty associated with the position measurements decreases. As also expected, in the excited state, the electrons are more weakly trapped by the harmonic potential. In turn, for more rigorous confinements ($\omega \to \infty$), the entropy sum becomes approximately constant. The entropic uncertainty relation (25), with $D = 6$, i.e., $S_t \geq 12.8684$, is satisfied for the spherical artificial helium atom.

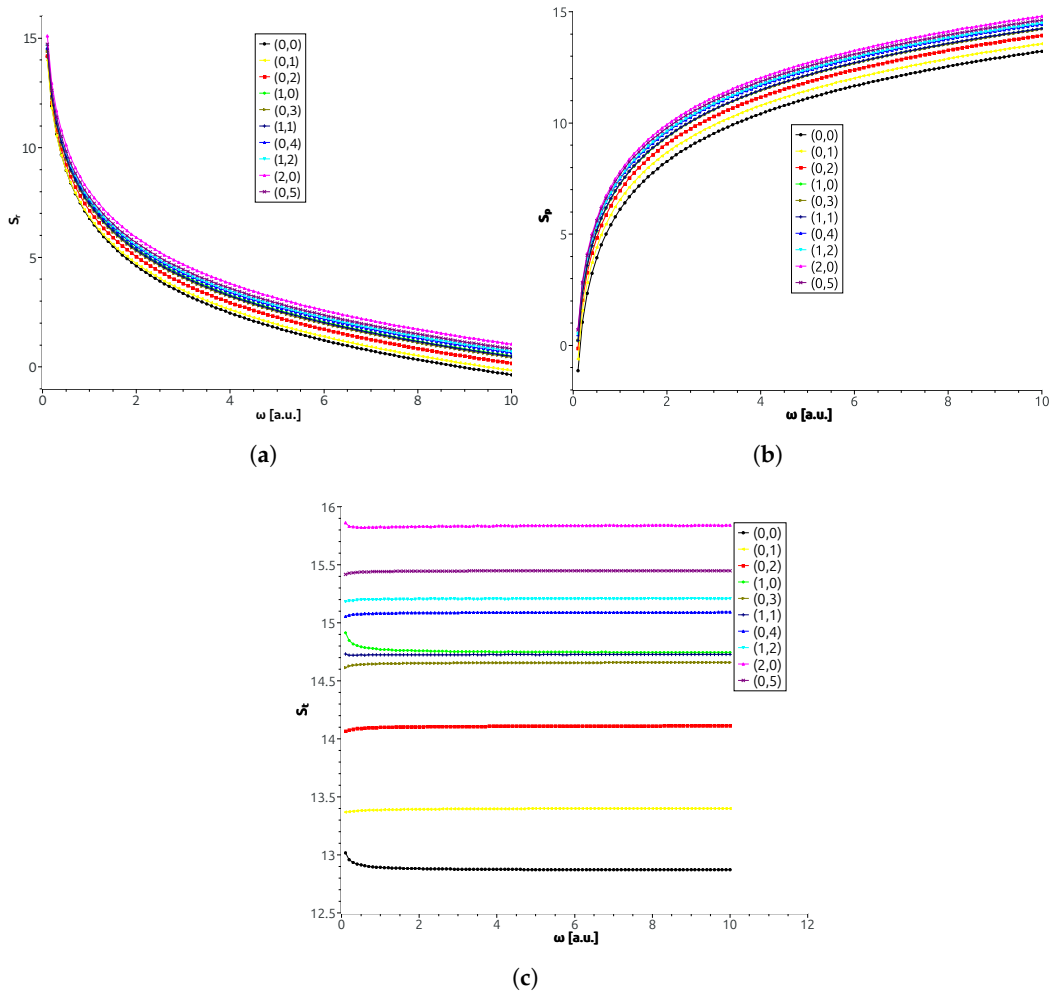

Figure 2. In (**a**) S_r, (**b**) S_p and (**c**) S_t entropies for different quantum states, (n, l), as a function of ω for the spherical artificial helium atom.

In Table 2 we highlight for presentation some values of S_r and S_p for different system states, (n,l), in ascending order of energy, with ω = 0.1, 0.5 and 4.0. We can see that the informational entropies for a fixed value of ω do not follow the monotonic increase behavior of the energy values.

We define here that ΔS_r are the S_r values of the spherical artificial helium atom minus the spherical artificial helium atom without Coulomb interaction. In Figure 3 we present the ΔS_r curves for different quantum states, (n,l), as a function of ω. We identified that ΔS_r tends to zero 0 when ω tends to infinity (increased confinement). This indicates that the Coulomb interaction potential between the electrons is no longer important for strong confinements and the system begins to behave as an independent particle model. It is also visible that the ground state is more influenced by the interaction potential when compared to other states, since it tends more slowly towards the behavior of two non-interacting particles. This behavior is in accordance with that indicated by Nascimento et al. [38].

Table 2. Informational entropies S_r and S_p for different system states, (n,l), with three different ω values for the spherical artificial helium atom.

	$\omega = 0.1$		$\omega = 0.5$		$\omega = 4.0$	
(n,l)	S_r	S_p	S_r	S_p	S_r	S_p
$(0,0)$	14.1564	−1.1391	8.9697	3.9425	2.4599	10.4151
$(0,1)$	13.9867	−0.6189	8.9695	4.4120	2.6151	10.7823
$(0,2)$	14.1879	−0.1239	9.2439	4.8475	2.9391	11.1698
$(1,0)$	14.7037	0.2114	9.6545	5.1396	3.2836	11.4654
$(0,3)$	14.3877	0.2264	9.4802	5.1598	3.1978	11.4571
$(1,1)$	14.5077	0.2218	9.5551	5.1674	3.2457	11.4798
$(0,4)$	14.5636	0.4904	9.6771	5.3993	3.4069	11.6820
$(1,2)$	14.6687	0.5136	9.7576	5.4410	3.4726	11.7336
$(2,0)$	15.0980	0.7638	10.1232	5.6979	3.8091	12.0280
$(0,5)$	14.7173	0.7004	9.8439	5.5929	3.5812	11.8660

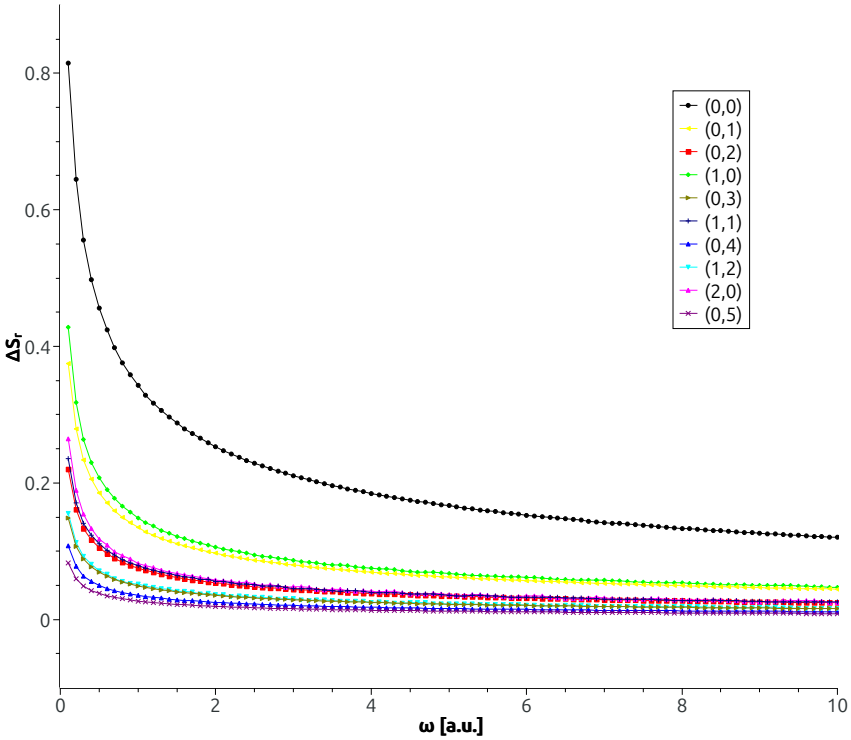

Figure 3. Values of ΔS_r for different quantum states, (n,l), as a function of ω for the spherical artificial helium atom.

3.2. Cylindrical Artificial Helium Atom

We examine here the cylindrical artificial helium (anisotropic case of the potential). In this scenario, we have $\omega_\perp \neq \omega_z$, being that, according to Equations (14) and (22), the quantum numbers that define the states of the movement of the center of mass are (N, M, N_z) and of the relative movement between the electrons are (n, m, n_z). Still, the coupling term, $A^m_{ll'}$ (Equation (21)), imposes the condition that every set of values of l must be either even (singlet state) or odd (triplet state).

Again, we present the results of the total energy, E, and S_r entropy for different states, (n, m, n_z), always in the ground state of the center of mass problem, $(N, M, N_z) = (0, 0, 0)$.

In Figure 4 we have the total energy, E, for different quantum states, (n, m, n_z), as a function of ω_z and fixing $\omega_\perp = 0.5$. We identified that, compared to the isotropic case, the band structure disappears when ω_z increases since the movement becomes governed by the harmonic potential whose associated energy spectrum has generally no degeneracy for values of n and n_z.

We noted that, between singlet (l even) and triplet (l odd) states (as discussed in Section 2.1 examining Equation (21)), crossings can occur, but not for states of the same parity and m value. Thus, avoided crossings appear between states of the same parity and projection of angular momentum. The occurrence of these avoided crossings reveals an oscillating behavior in the energy states, and the higher the energy level, the more persistent this oscillation. Similar behavior was obtained by Nascimento et al. [45] in the system of one electron confined in an asymmetric double quantum dot.

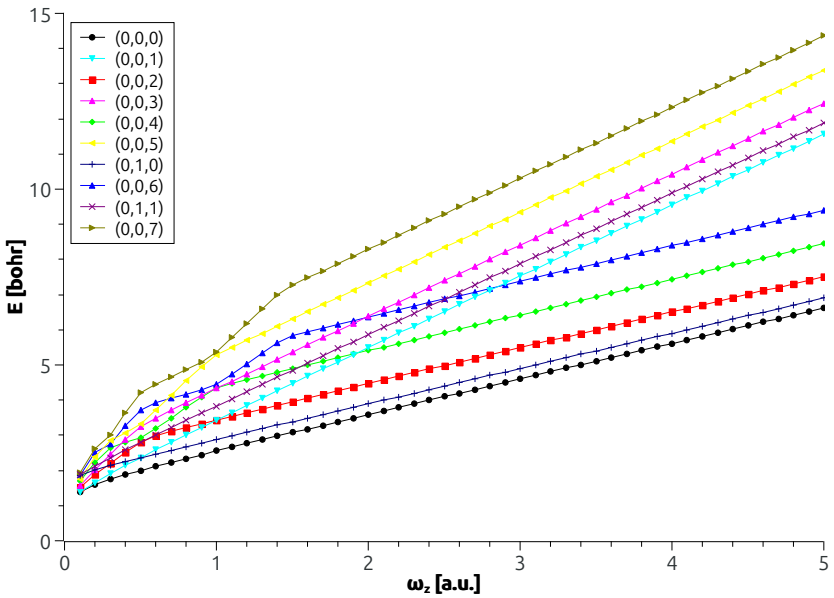

Figure 4. Total energy, E, for different quantum states, (n, m, n_z), as a function of ω_z for the cylindrical artificial helium atom ($\omega_\perp = 0.5$).

Interestingly, states of the same parity are obtained from the diagonalization of the same matrix, which led us to think that the avoided crossings could be false, resulting from a characteristic of the diagonalization algorithms that tend to order the eigenvalues in an increasing way. However, the analysis of the eigenvectors showed us that the ordering of the eigenvalues was correct, and the avoided crossings are, in fact, true. For example, in Figure 5 we show the radial density function, $|\Psi(r)|^2 = r^2 \int |\Psi_{RM}|^2 d\Omega$, in the second and third quantum states of even symmetry (with $m = 0$) for weak ($\omega_z = 0.1$) and strong ($w_z = 10.0$) confinements. As we can see, in fact, the functions maintained their waveform, that is, their number of peaks (local maxima) did not change, showing that, for these

two levels, the ordering of the eigenvalues is compatible with their eigenvectors. Similar analysis can be performed for other levels.

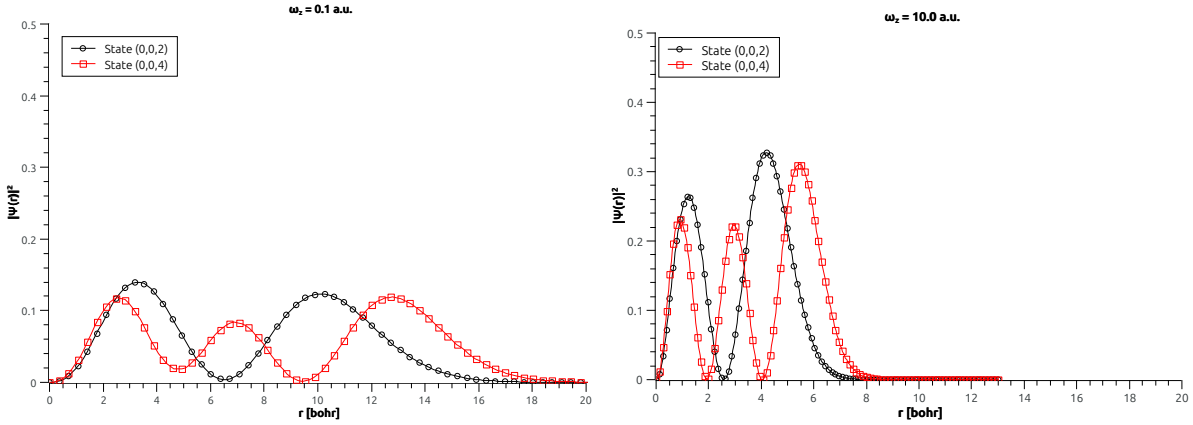

(**a**) (**b**)

Figure 5. Radial density function in second and third singlet quantum states for the confinements in (**a**) weak, $\omega_z = 0.1$, and (**b**) strong, $\omega_z = 10.0$ ($\omega_\perp = 0.5$).

In Figure 6 we present the informational entropy in position space for different system states, (n, m, n_z) as a function of ω_z with $\omega_\perp = 0.5$ fixed. In the graph (a) we have S_r versus ω_z for the even parity states and in the graph (b) S_r versus ω_z is for the odd parity states, both with quantum number m = 0. For each graph, there are only avoided crossings in the energy curves (see Figure 4) and the observed abrupt changes in behavior of S_r reflects this. We can see that in the ground state of each parity, namely $(0, 0, 0)$ and $(0, 0, 1)$, there is no abrupt change in behavior in S_r because these states do not have avoided crossings in the energy curves. On the other hand, in the first excited state of each parity, i.e., $(0, 0, 2)$ and $(0, 0, 3)$, an abrupt change in S_r occurs precisely at the location of the confinement value, w_z, where the avoided crossing happens in the energy curves. In the other excited states of each symmetry, changes occur in more than one location, since there are several locations where avoided crossings happen in the energy.

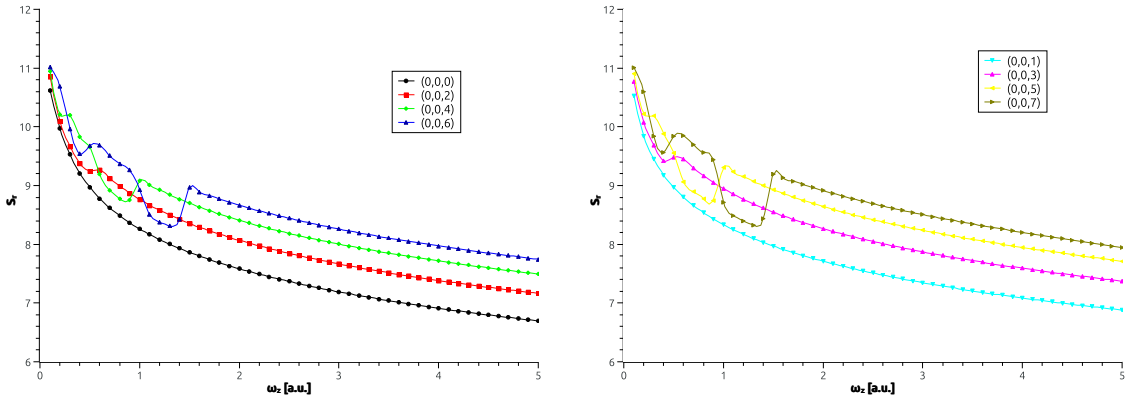

(**a**) (**b**)

Figure 6. In (**a**,**b**) values of S_r in different quantum states as a function of ω_z for the cylindrical artificial helium (with $\omega_\perp = 0.5$).

In Table 3 we organize, in ascending order of energy, the determined values of the informational entropy S_r for different system states, (n, m, n_z), with ω_z = 0.1, 1.0 and 4.0. As in the case of the spherical artificial helium atom, we can see that the S_r entropy does not follow the monotonic increase behavior of the energy values.

Table 3. Informational entropy S_r for different system states, (n, m, n_z), with three different ω_z values for the cylindrical artificial helium ($\omega_\perp = 0.5$).

$\omega_z = 0.1$		$\omega_z = 1.0$		$\omega_z = 4.0$	
(n, m, n_z)	S_r	(n, m, n_z)	S_r	(n, m, n_z)	S_r
$(0, 0, 0)$	10.6205	$(0, 0, 0)$	8.2612	$(0, 0, 0)$	6.9117
$(0, 0, 1)$	10.5241	$(0, 1, 0)$	8.5527	$(0, 1, 0)$	7.1609
$(0, 0, 2)$	10.8540	$(0, 2, 0)$	8.7503	$(0, 2, 0)$	7.3573
$(0, 0, 3)$	10.7673	$(1, 0, 0)$	8.7640	$(1, 0, 0)$	7.3840
$(0, 0, 4)$	10.9458	$(0, 0, 1)$	8.3347	$(0, 3, 0)$	7.5045
$(0, 0, 5)$	10.9072	$(0, 3, 0)$	8.8962	$(1, 1, 0)$	7.6054
$(0, 1, 0)$	11.2061	$(0, 1, 1)$	8.7798	$(0, 4, 0)$	7.6204
$(0, 0, 6)$	11.0205	$(1, 1, 0)$	9.0014	$(1, 2, 0)$	7.7588
$(0, 1, 1)$	11.0988	$(0, 4, 0)$	9.0109	$(2, 0, 0)$	7.7166
$(0, 0, 7)$	11.0079	$(1, 2, 0)$	9.1536	$(0, 5, 0)$	7.7154

In order to analyze in more detail what occurs in the regions of avoided crossings, in Figure 7 we show the evolution of the radial density function of the second and third quantum states with even symmetry and $m = 0$, namely, states $(0, 0, 2)$ and $(0, 0, 4)$, for different values of the confinement parameter ω_z (with $\omega_\perp = 0.5$). We analyze the behavior in an interval $\omega_z = [0.2, 1.0]$. In this interval, we see in Figure 4 that the state $(0, 0, 2)$ has an avoided crossing with the state $(0, 0, 4)$ around $\omega_z = 0.5$ and that, in turn, the state $(0, 0, 4)$ has other avoided crossings around $\omega_z = 0.3$ and $\omega_z = 1.0$. Having observed Figure 5a and continuing the observation in Figure 7a, we see the states $(0, 0, 2)$ and $(0, 0, 4)$ evolve with two and three peaks, respectively. However, as Figure 7b,c shows, the radial density functions are deformed, since they are approaching the avoided crossing regions around $\omega_z = 0, 3$, for $(0, 0, 4)$ states only, and $\omega_z = 0.5$, which acts as a kind of "barrier". In Figure 7d, the radial density functions of the states $(0, 0, 2)$ and $(0, 0.4)$ are found with one and two peaks, respectively. Then, following Figure 7e–i, we see that the state $(0, 0, 2)$ deforms in the sense of returning to having two peaks, since there is no other avoided crossing for this state. However, the state $(0, 0, 4)$ still does not return to having three peaks, since there is $\omega_z = 1.0$ an avoided crossing with a higher state. Therefore, the state $(0, 0, 4)$ still feels a second "barrier" before continuing "freely" in the direction of increased confinement. In Figure 5b we see that the state $(0, 0, 4)$ returns to having three peaks well after passing through the second "barrier". Therefore, the sudden changes in the behavior of the position entropy reflect the presence of this "barrier" encountered throughout the variation in quantum confinement.

We conclude that the avoided crossings correspond to abrupt changes in the information entropy S_r and, therefore, in the shape of the wave function, which can be verified by directly plotting some of these functions. The valleys in the entropy curves indicate a sudden concentration of the wave function, which means that for these specific values of the confinement parameter, the electrons in these states are particularly well-localized. We were able to conclude that, in the anisotropic case, the states of the system are especially sensitive to certain values of the confinement parameter. For large values of the confinement parameter, the wave functions return to their 'regular shape'.

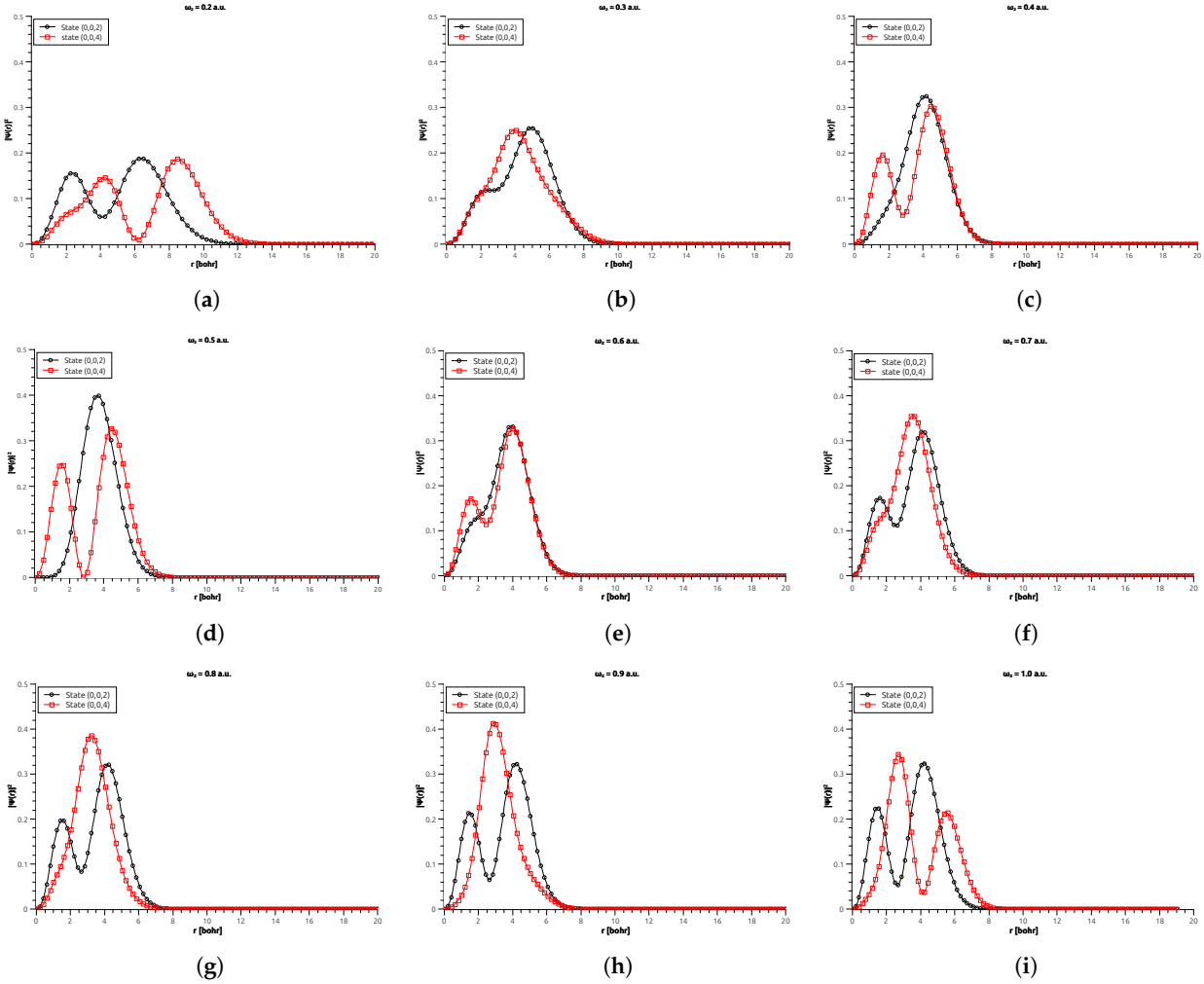

Figure 7. In graphs (**a**–**i**) we indicate the evolution of the radial density function in second and third singlet quantum states for different values of ω_z confining parameter (with $\omega_\perp = 0.5$).

4. Conclusions

In this work, we have studied, on the basis of the calculation of information entropy, the two-electron quantum dot confined by a three-dimensional harmonic potential. We have focused on the cases in which the potential has a spherical (isotropic) and a cylindrical (anisotropic) symmetry.

The results for the isotropic case showed that with increasing confinement intensity, the energy spectrum begins to present a band structure, resembling the degenerate spectrum of two non-interacting particles governed by a harmonic potential. As expected, the information entropy in position space tends to decrease as the confinement strength increases, which is simply interpreted as a decrease in the dispersion of the position measurements in the case where the particles are more strongly trapped by the potential. The information entropy in the momentum space, in turn, tends to increase with increasing confinement strength, indicating that the momentum measurements become more spread out.

In the anisotropic case, the band structure for the energies is not observed as sharply as in the previous case. The breaking of spatial symmetry gives rise to numerous avoided crossings between the energies of states with the same projection of the angular momentum. Similar effects on the information entropic curves are also analyzed in Ref. [45].

These results are interesting for defining the extent to which the interaction between electrons and the symmetry of confinement should be taken into account in real situations. A possible implication of our findings could be the study of the relationship between the

behavior of information entropies and the quantum entanglement of electrons. For example, the results of the isotropic case for the behavior of particles with increasing confinement intensity are consistent with the results obtained by other researchers concerning the behavior of quantum entanglement in two-electron systems [55,56]. It was found, among other things, that the quantum entanglement between two electrons tends to decrease when the strength of the confining potential increases, which means that the electrons tend to behave as independent (non-entangled) particles. In turn, for the anisotropic case, the results suggest that there may be interesting non-trivial effects related to the behavior of entanglement between two electrons when there is a symmetry transition in the confining potential.

Author Contributions: M.N.G., R.N.C., W.S.N. and F.V.P. contributed equally to this work. All authors have read and agreed to the published version of the manuscript.

Funding: This research received no external funding.

Data Availability Statement: Data are available from the authors after a reasonable request.

Acknowledgments: We acknowledge the partial financial support provided by the Brazilian "Coordenação de Aperfeiçoamento de Pessoal de Nível Superior" (CAPES)—Finance Code 001. R.N.C. is grateful to "Coordenação de Aperfeiçoamento de Pessoal de Nível Superior" (CAPES) for grants. F.V.P. is also grateful for the provision of computational time in the Centro Nacional de Computação (CESUP), Universidade Federal do Rio Grande do Sul. The authors thank the referees for careful reading of the manuscript and for helpful comments and suggestions.

Conflicts of Interest: The authors declare no conflicts of interest.

References

1. Knoss, R.W. (Ed.) *Quantum Dots Research, Technology and Applications*; Nova Science Publishers: New York, NY, USA, 2009.
2. Kastner, M.A. The single-electron transistor. *Rev. Mod. Phys.* **1992**, *64*, 849. [CrossRef]
3. Lee, Y.; Jun, H.; Park, S.; Kim, D.Y.; Lee, S. Transport Characteristics of Silicon Multi-Quantum-Dot Transistor Analyzed by Means of Experimental Parametrization Based on Single-Hole Tunneling Model. *Nanomaterials* **2023**, *13*, 1809. [CrossRef]
4. Wu, J.; Wang, Z.M. (Eds.) *Quantum Dot Solar Cells*; Springer: New York, NY, USA, 2014.
5. Cavassilas, N.; Suchet, D.; Delamarre, A.; Guillemoles, J.; Michelini, F.; Bescond, M.; Lannoo, M. Optimized Operation of Quantum-Dot Intermediate-Band Solar Cells Deduced from Electronic Transport Modeling. *Phys. Rev. Appl.* **2020**, *13*, 044035. [CrossRef]
6. Jang, E.; Jang, H. Review: Quantum Dot Light-Emitting Diodes. *Chem. Rev.* **2023**, *123*, 4663. [CrossRef] [PubMed]
7. Yu, R.; Yin, F.; Zhou, D.; Zhu, H.; Ji, W. Efficient Quantum-Dot Light-Emitting Diodes Enabled via a Charge Manipulating Structure. *J. Phys. Chem. Lett.* **2023**, *14*, 4548. [CrossRef]
8. Tóth, G.; Lent, C.S. Quantum computing with quantum-dot cellular automata. *Phys. Rev. A* **2001**, *63*, 052315. [CrossRef]
9. Jefferson, J.H.; Fearn, M.; Tipton, D.L.J.; Spiller, T.P. Two-electron quantum dots as scalable qubits. *Phys. Rev. A* **2002**, *66*, 042328. [CrossRef]
10. Chiquito, A.J. Pontos quânticos: Átomos artificiais e transistores atômicos. *Rev. Bras. Ensino Fis.* **2001**, *23*, 159. [CrossRef]
11. Bimberg, D.; Grundmann, M.; Ledentsov, N.N. *Quantum dot Heterostructures*; Wiley: Chichester, UK, 1999.
12. Ashoori, R.C. Electrons in artificial atoms. *Nature* **1996**, *379*, 413. [CrossRef]
13. Kastner, M.A. The single electron transistor and artificial atoms. *Ann. Phys.* **2000**, *512*, 885. [CrossRef]
14. Sako, T.; Diercksen, G.H.F. Confined quantum systems: A comparison of the spectral properties of the two-electron quantum dot, the negative hydrogen ion and the helium atom. *J. Phys. B At. Mol. Opt. Phys.* **2003**, *36*, 1681. [CrossRef]
15. Reimann, S.M.; Manninen, M. Electronic structure of quantum dots. *Rev. Mod. Phys.* **2002**, *74*, 1283. [CrossRef]
16. Maniero, A.; Prudente, F.; de Carvalho, C.; Jalbert, G. 3D two-electron double quantum dot: Comparison between the behaviour of some physical quantities under two different confinement potentials in the presence of a magnetic field. *Physica B* **2023**, *657*, 414818. [CrossRef]
17. Kouwenhoven, L.P.; Austing, D.G.; Tarucha, S. Few-electron quantum dots. *Rep. Prog. Phys.* **2001**, *64*, 701. [CrossRef]
18. Chan, I.H.; Fallahi, P.; Vidan, A.; Westervelt, R.M.; Hanson, M.; Gossard, A.C. Few-electron double quantum dots. *Nanotechnology* **2004**, *15*, 609. [CrossRef]
19. Alivisatos, A.P. Semiconductor Clusters, Nanocrystals, and Quantum Dots. *Science* **1996**, *271*, 933. [CrossRef]

20. Brauman, J.I. Clusters. *Science* **1996**, *271*, 889. [CrossRef]
21. Adamowski, J.; Sobkowicz, M.; Szafran, B.; Bednarek, S. Electron pair in a Gaussian confining potential. *Phys. Rev. B* **2000**, *62*, 4234. [CrossRef]
22. Kasapoglu, E.; Yücel, M.B.; Duque, C.A. Harmonic-Gaussian Symmetric and Asymmetric Double Quantum Wells: Magnetic Field Effects. *Nanomaterials* **2023**, *13*, 892. [CrossRef]
23. Maniero, A.M.; de Carvalho, C.R.; Prudente, F.V.; Jalbert, G. Effect of a laser field in the confinement potential of two electrons in a double quantum dot. *J. Phys. B At. Mol. Opt. Phys.* **2019**, *52*, 095103. [CrossRef]
24. Durak, S.; Sakiroglu, S. Theoretical investigation of laser field effect on nonlinear optical properties of quantum dots. *Physica B* **2023**, *650*, 414575. [CrossRef]
25. Maniero, A.M.; de Carvalho, C.R.; Prudente, F.V.; Jalbert, G. Oscillating properties of a two-electron quantum dot in the presence of a magnetic field. *J. Phys. B At. Mol. Opt. Phys.* **2020**, *53*, 185001. [CrossRef]
26. Chaudhuri, S. Two-electron quantum dot in a magnetic field: Analytic solution for finite potential model. *Physica E* **2021**, *128*, 114571. [CrossRef]
27. Plastino, A.R.; Plastino, A. Maximum entropy and approximate descriptions of pure states. *Phys. Lett. A* **1993**, *181*, 446–449. [CrossRef]
28. Shannon, C.E.; Weaver, W. *The Mathematical Theory of Communication*; Illini Books: Champaign, IL, USA, 1949.
29. Rioul, O. *Théorie de L'Information et du Codage*; Lavoisier: Paris, France, 2007.
30. Björk, G. Information gain when measuring an unknown qubit. *Eur. J. Phys.* **2018**, *39*, 015403. [CrossRef]
31. Ricotta, C. Bridging the gap between ecological diversity indices and measures of biodiversity with Shannon's entropy: Comment to Izsák and Papp. *Ecol. Modell.* **2002**, *152*, 1. [CrossRef]
32. Dabas, S.; Joshi, R. A numerical evaluation of Shannon entropy for modified Hulthen potential. *Eur. Phys J. D* **2022**, *76*, 95. [CrossRef]
33. Singh, S.; Saha, A. Shannon Information Entropy Sum of a Free Particle in Three Dimensions Using Cubical and Spherical Symmetry. *J. Sci. Res.* **2023**, *15*, 71. [CrossRef]
34. Santos, A.J.; Prudente, F.V.; Guimarães, M.N.; Nascimento, W.S. A Study of Strong Confinement Regions Using Informational Entropy. *Quantum Rep.* **2022**, *4*, 544–557. [CrossRef]
35. Salazar, S.J.C.; Laguna, H.G.; Dahiya, B.; Prasad, V.; Sagar, R.P. Shannon information entropy sum of the confined hydrogenic atom under the influence of an electric field. *Eur. Phys. J. D* **2021**, *75*, 127. [CrossRef]
36. Nascimento, W.S.; Prudente, F.V. Shannon entropy: A study of confined hydrogenic-like atoms. *Chem. Phys. Lett.* **2018**, *691*, 401. [CrossRef]
37. Estañón, C.R.; Montgomery, H.E., Jr.; Angulo, J.C.; Aquino, N. The confined helium atom: An information–theoretic approach. *Int. J. Quantum Chem.* **2024**, *124*, e27358. [CrossRef]
38. Nascimento, W.S.; de Almeida, M.M.; Prudente, F.V. Coulomb Correlation and Information Entropies in Confined Helium-Like Atoms. *Eur. Phys. J. D* **2021**, *75*, 171. [CrossRef]
39. Ou, J.H.; Ho, Y.K. Shannon Information Entropy in Position Space for the Ground and Singly Excited States of Helium with Finite Confinements. *Atoms* **2017**, *5*, 15. [CrossRef]
40. Verma, N.; Joshi, R. Shannon entropy for hydrogen atom in Debye and quantum plasma environment. *Phys. Plasmas* **2023**, *30*, 063905. [CrossRef]
41. Zan, L.R.; Jiao, L.G.; Ma, J.; Ho, Y.K. Information-theoretic measures of hydrogen-like ions in weakly coupled Debye plasmas. *Phys. Plasmas* **2017**, *24*, 122101. [CrossRef]
42. Shafeekali, H.; Olendski, O. Quantum-information theory of magnetic field influence on circular dots with different boundary conditions. *Phys. Scr.* **2023**, *98*, 085107. [CrossRef]
43. Liu, X.; Xie, X.; Wang, D.; Wang, C.; Zhao, Y.; Zhang, S. The effect of in-doping on the quantum information entropy of hydrogenic impurity states in the InxGa1-xN semiconductor quantum dot. *Philos. Mag.* **2023**, *103*, 892–913. [CrossRef]
44. Nascimento, W.S.; Maniero, A.M.; Prudente, F.V.; de Carvalho, C.R.; Jalbert, G. Electron confinement study in a double quantum dot by means of Shannon entropy information. *Physica B* **2024**, *677*, 415692. [CrossRef]
45. Nascimento, W.S.; Maniero, A.M.; Prudente, F.V.; de Carvalho, C.R.; Jalbert, G. Informational analysis of the confinement of an electron in an asymmetric double quantum dot. *Physica B* **2025**, *699*, 416769. [CrossRef]
46. González-Férez, R.; Dehesa, J.S. Shannon Entropy as an Indicator of Atomic Avoided Crossings in Strong Parallel Magnetic and Electric Fields. *Phys. Rev. Lett.* **2003**, *91*, 113001. [CrossRef]
47. González-Férez, R.; Dehesa, J.S. Characterization of atomic avoided crossings by means of Fisher's information. *Eur. Phys. J. D* **2005**, *32*, 39. [CrossRef]
48. Prudente, F.V.; Guimarães, M.N. Confined Quantum Systems Using the Finite Element and Discrete Variable Representation Methods. In *Electronic Structure of Quantum Confined Atoms and Molecules*; Sen, K.D., Ed.; Springer International Publishing: Oxford, UK, 2014; Chapter 5, p. 101. [CrossRef]

49. Sen, K.D. (Ed.) *Statistical Complexity: Applications in Electronic Struture*; Springer: Dordrecht, The Netherlands, 2011. [CrossRef]
50. Nascimento, W.S.; de Almeida, M.M.; Prudente, F.V. Information and quantum theories: An analysis in one-dimensional systems. *Eur. J. Phys.* **2020**, *41*, 025405. [CrossRef]
51. Corzo, H.H.; Laguna, H.G.; Sagar, R.P. Localization-delocalization phenomena in a cyclic box. *J. Math. Chem.* **2012**, *50*, 233. [CrossRef]
52. Bialynicki-Birula, I.; Mycielski, J. Uncertainty relations for information entropy in wave mechanics. *Commun. Math. Phys.* **1975**, *44*, 129. [CrossRef]
53. Prudente, F.V.; Costa, L.S.; Vianna, J.D.M. A study of two-electron quantum dot spectrum using discrete variable representation method. *J. Chem. Phys.* **2005**, *123*, 224701. [CrossRef]
54. Cordeiro, R.N. Sistemas de Dois Elétrons Confinados Harmonicamente Usando Coordenadas Hiperesféricas e Método do Elemento Finito. Master's Thesis, Physics Institute—Federal University of Bahia, Salvador, Brazil, 2022.
55. Manzano, D.; Plastino, A.R.; Dehesa, J.S.; Koga, T. Quantum entanglement in two-electron atomic models. *J. Phys. A Math. Theor.* **2010**, *43*, 275301. [CrossRef]
56. Nazmitdinov, R.G.; Simonović, N.S.; Plastino, A.R.; Chizhov, A.V. Shape transitions in excited states of two-electron quantum dots in a magnetic field. *J. Phys. B At. Mol. Opt. Phys.* **2012**, *45*, 205503. [CrossRef]